Optimal Placement of Electric Springs in Unbalanced Distribution Networks Using Improved Backward/forward Sweep Method Based Genetic Algorithm

Guillermo Tapia-Tinoco, Gerardo Humberto Valencia-Rivera, Martin Valtierra-Rodriguez, *Senior Member*, *IEEE*, Arturo Garcia-Perez, *Senior Member*, *IEEE*, and David Granados-Lieberman, *Senior Member*, *IEEE*

***Abstract*—A novel planning tool for optimizing the placement of electric springs (ESs) in unbalanced distribution networks is introduced in this study. The total voltage deviation is used as the optimization criterion and is calculated when the ESs operate at their maximum reactive power either in the inductive or capacitive modes. The power rating of the ES is adjusted on the basis of the available active power at the bus. And in the optimization problem, it is expressed as the power ratio of the non-critical load (NCL) and critical load (CL). The implemented ES model is flexible, which can be used on any bus and any phase. The model determines the output voltage from the parameters and operating conditions at the point of common coupling (PCC). These conditions are integrated using the backward/forward sweep method (BFSM) and are updated during power flow calculations. The problem is described as a mixed-integer nonlinear problem and solved efficiently using an improved BFSM-based genetic algorithm, which computes power flow and ES placement simultaneously. The effectiveness of this method is evaluated through testing in IEEE 13-bus and 34-bus systems.**

***Index Terms*—Electric spring, genetic algorithm, backward/forward sweep optimal placement, power flow, voltage deviation.**

Manuscript received: June 20, 2024; revised: October 25, 2024; accepted: November 14, 2024. Date of CrossCheck: November 14, 2024. Date of online publication: March 21, 2025.

This work was supported by Consejo Nacional de Humanidades, Ciencia y Tecnología (CONAHCYT)—México (No. 863547), the fellowship 2021-000001-01NACF-00604 given to the G. H. Valencia-Rivera; and the scholarships 175599, 64698, 253652, and 296574, given to G. Tapia-Tinoco, A. Garcia-Perez, D. Granados-Lieberman, and M. Valtierra-Rodriguez, respectively, through the Sistema Nacional de Investigadoras e Investigadores (SNII)-CONAHCYT-México.

G. Tapia-Tinoco is with ENAP-Research Group, University of Guanajuato, Irapuato, Mexico (e-mail: guillermo.tapia@enap-rg.org).

G. H. Valencia-Rivera is with School of Engineering and Sciences, Tecnologico de Monterrey, Monterrey, Mexico (e-mail: A00834075@tec.mx).

M. Valtierra-Rodriguez is with ENAP-Research Group, Faculty of Engineering, Autonomous University of Queretaro, San Juan del Río, Mexico (e-mail: martin.valtierra@enap-rg.org).

A. Garcia-Perez is with Electronic Engineering Department, University of Guanajuato, Salamanca, Mexico (e-mail: arturo@ugto.mx).

D. Granados-Lieberman (corresponding author) is with ENAP-Research Group, National Technological Institute of Mexico, ITS Irapuato, Irapuato, Mexico (e-mail: david.granados@enap-rg.org).

DOI: 10.35833/MPCE.2024.000649

I. Introduction

DISTRIBUTION networks have undergone significant evolution, transitioning from conventional systems characterized by unidirectional energy flow to active distribution networks. This transformation is driven by the increasing integration of advanced communication, control, and management technologies, as well as the need to adapt to the challenges posed by distributed generation, the growth of renewable energies, and changing consumer demands [1]. Distributed power generation is known to have a wide range of benefits such as enhancing the resilience of the power grid, reducing energy transmission losses, and providing flexibility for the integration of renewable energies [2]. However, the stochastic behavior of alternative energy sources presents challenges such as bidirectional power flows, energy supply-demand imbalances, and voltage regulation issues [3].

To overcome these challenges, several devices and management schemes have been implemented. Device-level proposals, such as the distributed flexible AC transmission systems, serve as alternatives for voltage regulation in the power grid [4]. In contrast, demand-side management adjusts active power consumption in the power grid to achieve a local supply-demand balance without compromising consumer comfort [5], [6].

Meanwhile, the electric spring (ES) has emerged as a fast-response option capable of altering the active and reactive power exchanged with the power grid, thereby addressing multiple issues simultaneously. Therefore, it has become possible to regulate the voltage, tackle renewable energy intermittence, and achieve an equilibrium between supply and demand with a single device [7].

Most research works on this topic focus on improving the power and control stages of a single ES to demonstrate its positive impact on various power quality indicators. However, the full potential of ESs lies in the deployment of multiple units throughout the power grid [8].

In this context, centralized [9], distributed [10], or two-level [11] control schemes have been developed to manage the collective operation of ESs [12]. Previous research works

demonstrate the advantages of the coordinated operation of ESs within power networks. However, the optimal placement and number of ESs are unknown. In addition, the assumption of one ES per bus is infeasible because of the complexity and cost involved. The optimal placement of devices in power networks plays a crucial role in ensuring efficient, safe, and reliable power grid operation with the minimum investment. Formulating an optimization problem with these characteristics is a huge challenge owing to the inherently nonlinear and highly nonconvex nature of power networks [13].

In this regard, metaheuristics have exhibited outstanding performance, showcasing their efficacy across various applications [14], including but not limited to the optimal placement of charging stations for electric vehicles [15], compensator devices [4], distributed generation [16], and energy storage systems [17].

The optimal placement of ESs in distribution networks was explored in two previous studies. In [18], a planning method was proposed to optimize the number, location, capacity, and type of ESs plugged into the distribution network. A mixed-integer nonlinear problem (MINLP) was formulated and solved using the natural aggregate algorithm. The optimal placement of ESs was analyzed considering distributed generation and traditional voltage regulators. In [19], an allocation model was proposed to determine the optimal placement and power ratings of ESs in a distribution network using the total voltage deviation as the optimization target. A mixed integer linear programming problem was formulated and solved using standard commercial software. The results of both previous studies suggested that the power of the noncritical load (NCL) and the location of the ESs in the farthest grid buses considerably affected the total voltage deviation. Nonetheless, these results were highly correlated to homogeneous load flows along with uniformly distributed NCL power rates. The power flow interchange between the ESs and the utility grid remained the same regardless of the bus location. Consequently, the reactive power injected at the buses of the farthest branches from the main bus had a great impact on voltage deviation, thus influencing the solution found by the optimization algorithm. These considerations did not apply to an unbalanced distribution network because the load at each bus was different and can even vary in each phase [20]. Notably, various simplifications and assumptions were made during network modeling in the aforementioned studies, affecting the accuracy of the results.

Simplified one-line diagram configurations under balanced conditions differ from those under real operating conditions, which include untransposed lines and unbalanced loads. Furthermore, the power flow method uses a linear approximation based on linearized distributed flow equations around the nominal voltage, thus simplifying power flow calculation at the expense of accuracy. In addition, ES models, represented as linear approximations or power equations, depend on NCL parameters and power. Although the implementation becomes easy because of the simplicity of the models, additional constraints become necessary to determine operating limits. However, these limits, determined by designers, may lead to ES operations outside permitted ranges or restrictions, thereby affecting the search space of the optimization model and yielding suboptimal or infeasible solutions. To address these shortcomings, a planning method that integrates ESs, the backward/forward sweep method (BFSM) solution model based on genetic algorithms (GAs), and a novel fitness function, is proposed for the optimal placement of ESs in unbalanced distribution networks. To the best of the author's knowledge, this is the first time that this method has been applied for optimal placement of ESs. The contributions of this study are as follows:

1) A comprehensive optimization model is proposed for optimal placement of ESs in unbalanced distribution networks. This robust and complete model accounts for all relevant possible scenarios, incorporating the nonlinear behavior of power flow equations, the nonlinear behavior attributed to untransposed lines and unbalanced loads, and the nonlinear operating characteristics of an ES in capacitive and inductive modes.

2) An MINLP is formulated and efficiently solved using an improved BFSM-based GA, which makes it possible to simultaneously calculate power flow and determine optimal placement of ESs in unbalanced distribution networks.

3) The ratio of NCL and critical load (CL), i.e., *NCL*/*CL*, is implemented as a control variable within the optimization algorithm, which is constrained by the available active power at the bus and connection phases. Thus, the nominal power at the bus remains relatively unchanged, enabling the evaluation of the placements of ESs and the impact of the maximum reactive power on voltage deviation.

II. Steady-state ES Model Applied to Unbalanced Distribution Networks

The ES is a state-of-the-art device that has emerged as a viable alternative to address the challenges associated with active distribution networks. In an ES, a power converter is connected in series with a constant impedance NCL (Z_{NCL}). Examples of such loads include water heaters, air conditioners, and lighting systems, known for their ability to tolerate certain levels of voltage fluctuations. This innovative configuration is known as a smart load (SL), which enables the exchange of active and reactive power with the grid. The power rating and operational limits of the SL depend closely on the ES output voltage ($\boldsymbol{V}_{ES}$) and Z_{NCL}. To analyze the impact of these two parameters on the optimal placement of ESs within unbalanced distribution networks, an ES model of the connection to the bus is proposed, as shown in Fig. 1. Note that in Fig. 1, subscripts *m* and *n* denote the bus *m* and bus *n*, respectively; and the superscript *abc* denotes the three phases. The model includes input parameters as the impedances (Z_{mn}^{abc}) and susceptances (B_n^{abc} and B_m^{abc}) of the distribution line, the admittances of CLs ($Y_{ZIP_n}^{abc}$), and the impedances of NCLs (Z_{NCL}^{abc}). To simulate the CL at bus *n*, the loads are represented as ZIP_n loads (constant-impedance, constant-current, and constant-power loads), which is commonly employed to model loads in unbalanced distribution networks. Additionally, three single-phase ES units with voltages $\boldsymbol{V}_{ES_n}^{abc}$

are strategically distributed across the bus phases, and their connection/disconnection is controlled via switches (S_n^{abc}). The ES is modeled as an ideal voltage source, assuming negligible converter losses and efficient fundamental component extraction through filtering processes. The operating conditions in the ES model are provided by the BFSM. It includes the three-phase voltages at the buses ($\boldsymbol{V}_n^{abc}$ and $\boldsymbol{V}_m^{abc}$), the currents in the NCLs ($\boldsymbol{I}_{NCL_n}^{abc}$), and the operating conditions of the rest of the network, defined by the admittances ($Y_{Z_{no}}^{abc}$) and the currents ($\boldsymbol{I}_{Z_{no}}^{abc}$), where the subscript o denotes the bus o.

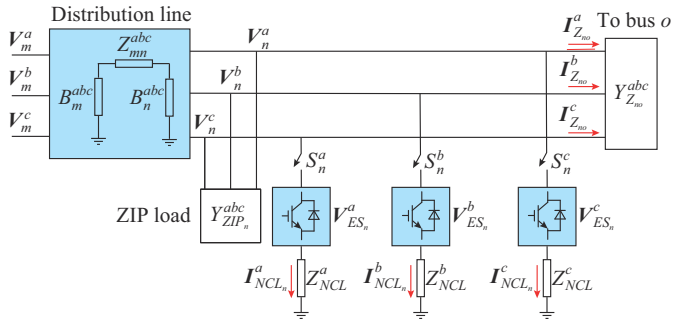

Fig. 1. Electric circuit of ES model contemplated in this study.

In [21], the procedure for establishing a steady-state model of an ES is detailed. This model is represented by (1)-(9) and is derived by examining the geometric relationships among the phasors and parameters of the elements involved in the bus connection. The subscripts in these equations denote the bus, whereas the superscripts indicate the connection phase. When the ES is placed in phase a, the following substitutions are made: $p=a$, $q=b$, and $r=c$. If the ES is positioned in phase b, the substitutions are as follows: $p=b$, $q=c$, and $r=a$. Lastly, if the ES is placed in phase c, the substitutions are $p=c$, $q=a$, and $r=b$. These equations are applicable to both single-phase and two-phase feeders. The adjustment is to eliminate the terms in the equations that carry superscripts associated with phases that do not exist in the feeder. The model is computed by the BFSM, which simultaneously calculates the power flow in the network and iteratively adjusts the angle of each ES (θ_n^p). This angle is computed based on $\boldsymbol{V}_{ES_n}^p$, the operating mode ($OM=1$ for inductive mode and $OM=-1$ for capacitive mode), and the voltage at the PCC ($\boldsymbol{V}_n^p$). This angle ensures that the ES operates in the reactive power compensation mode and allows for the calculation of the NCL current ($I_{NCL_n}^p$), as shown in (2). This current is injected by the SL at the connecting bus and is used in the backward sweep process of the BFSM.

$$\theta_n^p = 2\sin^{-1}\left(OM\,\frac{\boldsymbol{V}_{ES_n}^p}{\boldsymbol{V}_n^p}\right) \tag{1}$$

$$I_{NCL_n}^p = \frac{\boldsymbol{V}_n^p}{R_n^p}\cos\left(\frac{\theta_n^p}{2}\right) \tag{2}$$

where R_n^p is the resistance of the CL.

The angle θ_{lim} determines the operating limit of the ES and is calculated using (3), and its absolute value must not exceed $\pi/2$. If this limit is exceeded, $\boldsymbol{V}_{ES_n}^p$ is adjusted to the maximum allowable value, as shown in (3). The terms $V_{G1_n}^p$, φ_{1n}^p, φ_{0n}^p, K_n^p, a_n^p, and b_n^p are variables used to simplify the model representation, and they are calculated using (4)-(9).

$$\theta_{lim} = \theta_n^p + \tan^{-1}\left(\frac{b_n^p}{a_n^p}\right) \tag{3}$$

$$V_{G1_n}^p = V_n^p\left|1 + Z_{mn}^p\left(\mathrm{j}B_n^{pp} - \mathrm{j}B_n^{pq}\frac{\boldsymbol{V}_n^q}{\boldsymbol{V}_n^p} - \mathrm{j}B_n^{rp}\frac{\boldsymbol{V}_n^r}{\boldsymbol{V}_n^p} + \ldots + Y_{ZIP_n}^p + Y_{Z_{no}}^p\right)\right| \tag{4}$$

$$\varphi_{1n}^p = 1 + \arg\left(Z_{mn}^p\left(\mathrm{j}B_n^{pp} - \mathrm{j}B_n^{pq}\frac{\boldsymbol{V}_n^q}{\boldsymbol{V}_n^p} - \mathrm{j}B_n^{rp}\frac{\boldsymbol{V}_n^r}{\boldsymbol{V}_n^p} + \ldots + Y_{ZIP_n}^p + Y_{Z_{no}}^p\right)\right) \tag{5}$$

$$\varphi_{0n}^p = \tan^{-1}\left(\frac{X_{mn}^p}{R_{mn}^p}\right) \tag{6}$$

$$K_n^p = \sqrt{(R_{mn}^p)^2 + (X_{mn}^p)^2} \tag{7}$$

$$a_n^p = \frac{V_{G1_n}^p V_n^p}{R_n^p}K_n^p\cos(\varphi_{0n}^p + \varphi_{1n}^p) \tag{8}$$

$$b_n^p = \frac{1}{2}\left(\frac{V_n^p K_n^p}{R_n^p}\right)^2 + \frac{V_{G1_n}^p V_n^p}{R_n^p}K_n^p\sin(\varphi_{0n}^p + \varphi_{1n}^p) \tag{9}$$

where Z_{mn}^p, R_{mn}^p, and X_{mn}^p are the impedance, resistance, and reactance of the distribution line, respectively; B_n^{pp} is the self-susceptance of the distribution line; B_n^{pq} and B_n^{rp} are the mutual susceptances of the distribution line; $Y_{ZIP_n}^p$ is the admittance of the CL; $Y_{Z_{no}}^p$ is the admittance associated with the rest of the network; and $\boldsymbol{V}_n^q$ and $\boldsymbol{V}_n^r$ are the phase voltages.

III. Theoretical Foundation of ES Operating in Unbalanced Distribution Networks

In this section, we perform a phasor analysis of a symmetric distribution grid operating with and without ESs. To conduct this analysis, we utilize the power network in Fig. 1, where the voltage drop along the distribution line is determined by (10). The model incorporates the voltages at both ends of the distribution line ($\boldsymbol{V}_m^a$, $\boldsymbol{V}_m^b$, $\boldsymbol{V}_m^c$, $\boldsymbol{V}_n^a$, $\boldsymbol{V}_n^b$, and $\boldsymbol{V}_n^c$), along with the voltage drops attributed to its self-impedances ($Z_{mn}^{aa}\boldsymbol{I}_{Zmn}^a$, $Z_{mn}^{bb}\boldsymbol{I}_{Zmn}^b$, and $Z_{mn}^{cc}\boldsymbol{I}_{Zmn}^c$) and mutual impedances ($Z_{mn}^{ac}\boldsymbol{I}_{Zmn}^c$, $Z_{mn}^{ba}\boldsymbol{I}_{Zmn}^a$, $Z_{mn}^{bc}\boldsymbol{I}_{Zmn}^c$, $Z_{mn}^{ca}\boldsymbol{I}_{Zmn}^a$, and $Z_{mn}^{cb}\boldsymbol{I}_{Zmn}^b$).

$$\begin{cases} \boldsymbol{V}_m^a = Z_{mn}^{aa}\boldsymbol{I}_{Zmn}^a + Z_{mn}^{ab}\boldsymbol{I}_{Zmn}^b + Z_{mn}^{ac}\boldsymbol{I}_{Zmn}^c + \boldsymbol{V}_n^a \\ \boldsymbol{V}_m^b = Z_{mn}^{ba}\boldsymbol{I}_{Zmn}^a + Z_{mn}^{bb}\boldsymbol{I}_{Zmn}^b + Z_{mn}^{bc}\boldsymbol{I}_{Zmn}^c + \boldsymbol{V}_n^b \\ \boldsymbol{V}_m^c = Z_{mn}^{ca}\boldsymbol{I}_{Zmn}^a + Z_{mn}^{cb}\boldsymbol{I}_{Zmn}^b + Z_{mn}^{cc}\boldsymbol{I}_{Zmn}^c + \boldsymbol{V}_n^c \end{cases} \tag{10}$$

Figure 2 illustrates the phasor diagram corresponding to (10) without the operation of ESs, serving as the base case. The phase voltages at bus m are presumed to remain constant, possessing equal magnitudes and three-phase sequence. The magnitude of these voltages is represented in the figure by the outer circle with radius $|V_m|$. It is assumed that a balanced load and identical power factor are present in each phase of bus n. As a consequence of these operating

conditions, $\boldsymbol{I}^{a}_{Zmn}$, $\boldsymbol{I}^{b}_{Zmn}$, and $\boldsymbol{I}^{c}_{Zmn}$ exhibit identical magnitudes and three-phase angles, denoted as φ_a, φ_b, and φ_c. For simplicity, we assume that the distribution line is symmetric, with self-impedances of greater magnitude than mutual impedances. In the figure, it is evident that despite the line symmetry, the voltage drops associated with self-impedances exhibit a greater magnitude compared with the voltage drops of mutual impedances (as indicated by dashed components in black). Under these operating conditions, uniform voltage drops occur across each phase, resulting in the voltages at bus n having the same magnitude, as denoted by the circle of radius $|V_n|$. It can be observed that under these operating conditions, with an unbalanced load, the phase currents are no longer identical. Consequently, the voltage drops in each phase of the distribution line differ, leading to imbalances in the voltages at bus n. Furthermore, if an asymmetrical distribution line is considered, the imbalance will be higher.

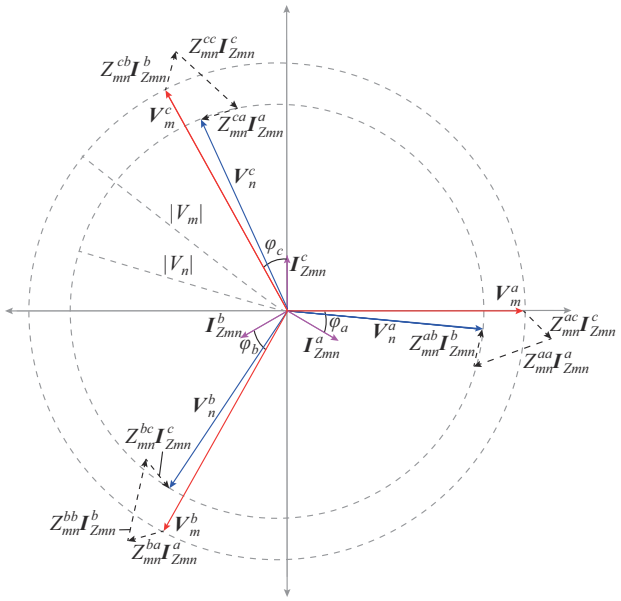

Fig. 2. Phasor diagram corresponding to (10) without operation of ESs.

The phasor diagram in Fig. 3 illustrates the operation under the same conditions as the base case, with the addition of a single-phase ES in phase a, operating in capacitive mode, alongside a resistive NCL. It is essential to emphasize that in this analysis, only a single-phase ES is employed to clearly observe its impact on the phasor diagram. However, the simulation model offers the flexibility to incorporate either single-phase ES or a three-phase ES, depending on the feeder type and the NCL available at the connection bus. In Fig. 3, it is evident that the inclusion of the ES affects $\boldsymbol{I}^{a}_{Zmn}$, while $\boldsymbol{I}^{b}_{Zmn}$ and $\boldsymbol{I}^{c}_{Zmn}$ remain unchanged. This alteration in $\boldsymbol{I}^{a}_{Zmn}$ leads to a reduction in the voltage drop across the elements in which it is involved (as depicted by components in solid black color). By maintaining the voltage drops associated with $\boldsymbol{I}^{b}_{Zmn}$ and $\boldsymbol{I}^{c}_{Zmn}$ unchanged, it becomes apparent that the voltages at bus n must be adjusted to comply with the model outlined in (10). Under these specific operating conditions, $\boldsymbol{V}^{a}_{n}$ increases in magnitude, whereas $\boldsymbol{V}^{b}_{n}$ and $\boldsymbol{V}^{c}_{n}$ decrease, with $\boldsymbol{V}^{b}_{n}$ experiencing the most significant decrease. Meanwhile, the NCL voltage ($\boldsymbol{V}^{a}_{NCL_n}$) leads $\boldsymbol{V}^{a}_{ES_n}$ by 90°, demonstrating the capacitive operation mode of the ES.

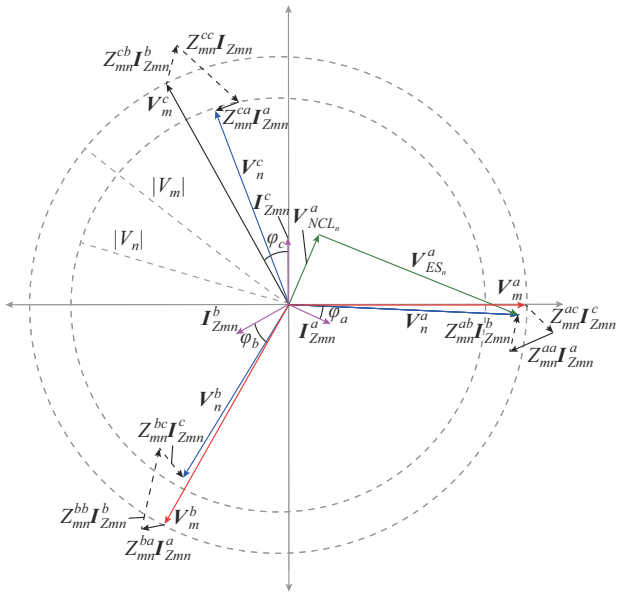

Fig. 3. Phasor diagram with a single-phase ES in capacitive mode.

In Fig. 4, the phasor diagram is shown under the same conditions as the base case, with a single-phase ES in inductive mode. Under these operating conditions, $\boldsymbol{V}^{a}_{NCL_n}$ lags $\boldsymbol{V}^{a}_{ES_n}$ by 90°, allowing the ES to absorb reactive power. The introduction of the ES in inductive mode results in an increase in both the magnitude and phase angle of $\boldsymbol{I}^{a}_{Zmn}$ compared with that of the base case. This change in $\boldsymbol{I}^{a}_{Zmn}$ leads to a corresponding increase in its associated voltage drops across the distribution line (as depicted by components in solid black color). It is apparent from the phasor diagram that the augmentation in voltage drops causes a decrease in voltage $\boldsymbol{V}^{a}_{n}$ and an increase in $\boldsymbol{V}^{b}_{n}$ and $\boldsymbol{V}^{c}_{n}$.

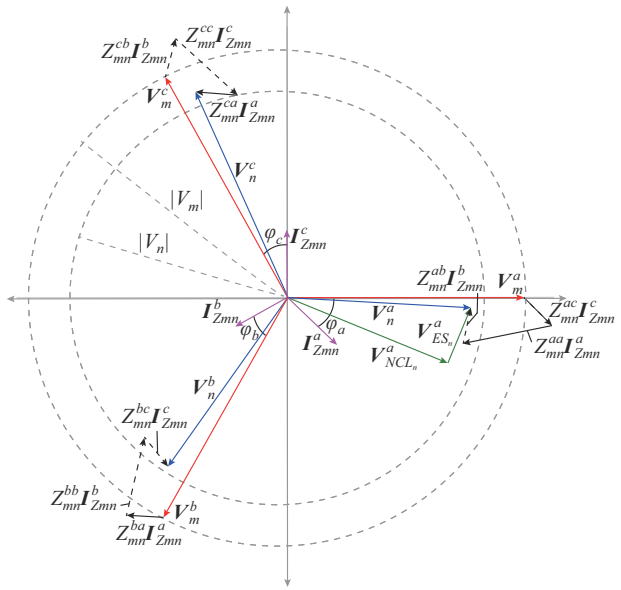

Fig. 4. Phasor diagram with a single-phase ES in inductive mode.

With regards to the SL, it is noticeable that for both operation modes, the total of their voltages equals $\boldsymbol{V}_n^a$. Moreover, it is evident that the operation not only affect the reactive power exchanged with the grid, but also alters its active power consumption by modifying $\boldsymbol{V}_{NCL_n}^a$. This characteristic of adjusting both active and reactive power distinguishes it from other compensating devices that solely control reactive power exchange, which expands the SL capability to regulate voltage and execute demand-side management tasks. Regarding the operating limits of the ES, these are defined by (3), and they are iteratively adjusted by the BFSM during the power flow calculation. This adjustment considers the operating conditions and parameters at the point of common coupling (PCC). From the preceding analysis, it can be inferred that the integration of an ES into a distribution network yields a global impact. The influence of the ES on nodal voltages is contingent upon its placement, power ratings, and operation mode. Moreover, the symmetry of the distribution line and the extent of load imbalance connected at the PCC also contribute to its effects.

IV. Proposed Method

The method outlined in Section II encompasses various key concepts. Among these, ESs, power quality (voltage deviation), and optimal placement are of paramount importance. ESs are directly related to the application at hand, whereas the others are the targets of the optimization problem. The optimization problem seeks to evaluate the influence of power levels and the strategic placement of ESs on the total voltage deviation within the distribution network. Direct consideration of investment costs is omitted from the objective function, as these costs are implicitly integrated into the constraints, owing to the inherent correlation between the cost of power converters and their power ratings. To provide a solution for this problem, metaheuristics are explored in this work due to their proven versatility and success in other power system applications [22]. This research work detects that the top three metaheuristics for optimizing these systems are particle swarm optimization, GAs, and grey wolf optimizer. GAs have been identified as the most suitable method for minimizing the fitness function presented in (13) due to several key factors. Firstly, the effectiveness in navigating large and complex search spaces helps avoid local minima, which is a common challenge in unbalanced distribution networks. Additionally, the inherent diversity of GA populations promotes a comprehensive exploration of potential solutions, increasing the likelihood of achieving global optimization. Preliminary performance tests, not detailed in this work for brevity, further demonstrate that GAs consistently outperform other metaheuristics in terms of convergence speed and robustness. This is supported by existing literature, where GAs, employed for at least 30 years, have been successfully applied to similar optimization problems in electrical engineering, showing superior adaptability to nonlinear and multifaceted fitness functions and effective integration of complex operational constraints [21], [23], [24].

A. GAs

A GA is a population-based solver that seeks to replicate the natural selection procedure by means of three genetic operators: selection, crossover, and mutation [25]. The first operator detects individuals who can provide genetic material for the next generations. The second operator merges the genetic material of the current population, and the last operator introduces genetic diversity by randomly altering some individuals.

Parent selection mechanisms have been extensively studied. For practicality, the roulette wheel selection method is used. This method is based on the probability of selecting the best chromosomes considering their fitness. Because the proposed method is a continuous problem, the crossover and mutation operators are coded for real-valued genomes. Therefore, the crossover is described as:

$$\boldsymbol{x}_c = \boldsymbol{r}_u \boldsymbol{x}_{p,1} + (1 - \boldsymbol{r}_u)\boldsymbol{x}_{p,2} \tag{11}$$

where $\boldsymbol{x}_c$ is the position of a child; $\boldsymbol{x}_{p,1}$, $\boldsymbol{x}_{p,2}$ is a pair of progenitors selected from the current population; and $\boldsymbol{r}_u$ is a vector of independent and identically distributed random numbers with uniform distribution $\mathcal{U} \in [0, 1]$. The mutation operator is arithmetically defined as:

$$\boldsymbol{x}_m = \boldsymbol{x}_1 + \alpha_m (\boldsymbol{x}_2 - \boldsymbol{x}_3) \tag{12}$$

where $\boldsymbol{x}_m$ is the resulting version of the mutated individual; $\boldsymbol{x}_i$ $(\forall i = 1, 2, 3)$ corresponds to three random different numbers between [0, 1]; and $\alpha_m \in [0, 1]$ is the percentage of information to mutate for each element in the chromosome.

B. Fitness Function

The chosen fitness function minimizes the voltage deviation of two unbalanced models of distribution networks through the strategic interconnection of a set of ESs. Moreover, this fitness function is based on a sequential method. Initially, it calculates the overall voltage deviation resulting from the ESs in capacitive mode. Subsequently, it evaluates the total voltage deviation attributed to the inductive mode of ESs. In addition, it considers three operational constraints on the distribution network, which are detailed later. Note that the optimization of voltage deviation for the ESs operating in one mode does not adversely affect the other mode. Therefore, a multi-objective method, including Pareto front analysis, is unnecessary. Besides, the proposed fitness function is integrated into a single-level problem for computational simplicity, preserving the integrity of the model. The objective function is defined as follows:

$$f(\boldsymbol{x}) = w_1 D_1 + w_2 D_2 + \sum_{k=1}^{n} \rho_k \gamma_k \tag{13}$$

where $w_1, w_2 \in [0, 1]$ are the designated weights for prioritizing the voltage deviation when the entire set of ESs plugged into the power grid operates in capacitive (D_1) or inductive (D_2) mode; and $\sum_{k=1}^{n} \rho_k \gamma_k$ is the penalty function, and γ_k can vary between 0 or 1 if the constraint k is violated, ρ_k is the optimization problem constraints, and n is the number of restrictions. For equal prioritizing both voltage deviations, w_1 and w_2 are set to be 0.5. Such voltage deviations are calculat-

ed using the following expression:

$$D_{1,2}=\frac{\sum(1-|\boldsymbol{V}_{bus}|)}{N_{buses}} \tag{14}$$

where subscript 1, 2 indicates the operation mode of the ESs, i.e., capacitive mode and inductive mode, respectively; $\boldsymbol{V}_{bus}$ is the voltage of all the buses in the distribution network; and N_{buses} is the number of buses. For this particular application, a maximum of four placements of the available bus positions at the distribution models is assumed. To avoid the operation of ESs outside the allowed constraints, which may lead to unfeasible solutions, the proposed fitness function is complemented with $\sum_{k=1}^{n}\rho_k\gamma_k$. The following optimization problem has three constraints, i.e., $n=3$, which are modeled as (15). The first two constraints correspond to the minimum voltage allowed by the NCL in both the capacitive and inductive modes. These constraints are calculated as the ratio of the voltage at buses with ES ($\boldsymbol{V}_{NCL_{1,2}}$) and the voltage at buses without ES installed ($\boldsymbol{V}_{1,2}$). A lower limit of 0.9 is selected based on thresholds proposed in [10], [26], [27], which typically fall within the range of 0.7 to 1.2. The third constraint defines the maximum limit of reactive power delivered by all ESs. The variable Q_{base} sets the base reactive power, whereas Q_t is a per-unit value that determines the threshold for the ES in the capacitive mode (Q_{ES_1}) and inductive mode (Q_{ES_2}).

$$\rho_k=\begin{cases}\left|\dfrac{\boldsymbol{V}_{NCL_1}}{\boldsymbol{V}_1}\right|\times 0.9\\ \left|\dfrac{\boldsymbol{V}_{NCL_2}}{\boldsymbol{V}_2}\right|\times 0.9\\ \left|Q_{ES_1},Q_{ES_2}\right|Q_tQ_{base}\end{cases} \tag{15}$$

V. Methodology for BFSM-based GA

The effects of connecting ESs in IEEE 13-bus and 34-bus systems are analyzed. These effects are manifested in one power quality metric: the total voltage deviation of the power grid. The flowchart of the methodology is shown in Fig. 5 to explain the method that solves the optimization problem. To complement the proposed method, a comprehensive statistical analysis is performed because the implemented optimizer, i.e., GA, uses random exploration to achieve an optimal solution. These statistical tests will be described in the following sections.

Figure 5(a) shows the GA flowchart for finding optimal placement of ESs. The process begins by randomly generating the entire population, which contains the chromosomes of each individual (potential solutions). The proposed optimization problem is based on an MINLP method. The size of the chromosome in each case study is determined by the variable m, which is associated with the number of ESs established in the optimal placement scheme. Each chromosome consists of two real variables ($\boldsymbol{NCLP}_{1\times m}$ and $\boldsymbol{VES}_{1\times m}$) and one discrete variable ($\boldsymbol{P}_{1\times m}$). ***NCLP*** determines the percentage of active power allocated to the NCLs at the connecting bus. ***VES*** establishes the output voltages of the ESs with reference to the nominal voltage in the distribution network. ***P*** determines the placement of the ES within the distribution network. These potential solutions are stored in the variable $\boldsymbol{X}_{n\times 3m}$. The objective is to evaluate each one of the solutions in the distribution network. For this purpose, the extract solution block is introduced for sending the generated solutions individually to the green-dotted block.

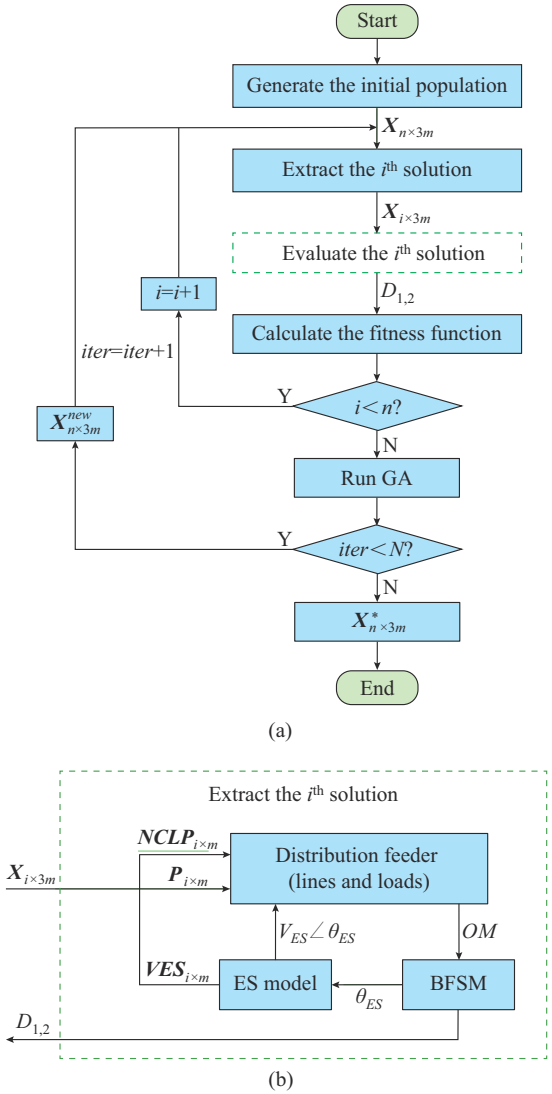

Fig. 5. Proposed BFSM-based GA. (a) GA flowchart for finding optimal placement of ES. (b) Power flow evaluation through BFSM.

Figure 5(b) is an extension of Fig. 5(a), which emphasizes the calculation of the total voltage deviation by the green-dotted block when the ESs are plugged into the distribution network benchmarks. This block receives the optimization problem variables. ***NCLP*** and ***P*** are transferred directly to the distribution network model, whereas ***VES*** passes through the ES model block because it depends on the phase angle setting ($V_{ES}\angle\theta_{ES}$). Here, the BFSM performs a twofold function. The first one is to set the ES phase angle (θ_{ES}), while the second one is to compute the power flow and subse-

quently calculate the total voltage deviations driven by D_1 and D_2 modes. Following the analysis shown in Fig. 5(a), the quality of the entire set of potential solutions is then measured through the proposed fitness function (13) in terms of voltage deviation minimization and problem constraint fulfillment. In this step, the genetic operators are applied to introduce diversity to the current solutions ($\boldsymbol{X}_{n\times 3m}$), thereby generating new solutions ($\boldsymbol{X}^{new}_{n\times 3m}$). If the number of iterations (*iter*) is achieved, the flowchart provides the optimal solution ($\boldsymbol{X}^{*}_{n\times 3m}$). Conversely, the GA-based methodology remains iterative. Note that GA is based on stochastic searching, implying that it may present different results in each run. Therefore, each experiment is replicated 31 times per ES configuration to evaluate the reliability of the obtained results. Thus, 124 possible solutions are obtained for each threshold value of Q_t in each of the distribution networks.

Table I summarizes the GA parameters considered in this study. These parameters are the same for both power grid topologies, excluding the number of available placements to connect the ESs. In the case of the IEEE 13-bus system, 12 possible placements exist, whereas the IEEE 34-bus system has 24 coupling points, as shown in Fig. 6. The potential locations are identified at the buses in Fig. 6 by markers in red, green, and blue hues, corresponding to phases *a*, *b*, and *c*, respectively. Each potential placement in the power networks shown in Fig. 6 corresponds to a single-phase ES. In the case of three-phase feeders, three single-phase ESs are considered (as illustrated in Fig. 1). These three single-phase ESs can collectively form a three-phase unit only if the NCL in each phase is identical. Nevertheless, they are treated as three independent ESs by the optimization algorithm. The allocation criteria are based on three-phase feeders with star-connected loads and single- and two-phase feeders with ground-connected loads. Therefore, it is feasible to implement the SL topology, as shown in Fig. 1. For the GA parameters, an initial population of 25 agents, a maximum iteration number of 50, and a random probability of crossover and mutation between 0 and 1 are considered. Nonetheless, after some exhaustive tests, we find that the GA configuration that provides the most satisfactory outcomes is the one indicated in Table I. Even though the GA never surpasses such a number of iterations, such a parameter performs as fail-safe if GA does not converge. The lower and upper bounds of VES and NCLP, as shown in rows 3 and 4 of Table I, are adopted following a previous study [28].

TABLE I
GA PARAMETERS CONSIDERED IN THIS STUDY

Parameter	Value
Population size	50
Iteration	100
Lower bounds of VES and NCLP (p.u.)	0.1, 0.1
Upper bounds of VES and NCLP (p.u.)	0.6, 0.7
Crossover ratio	0.8
Mutation ratio	0.3

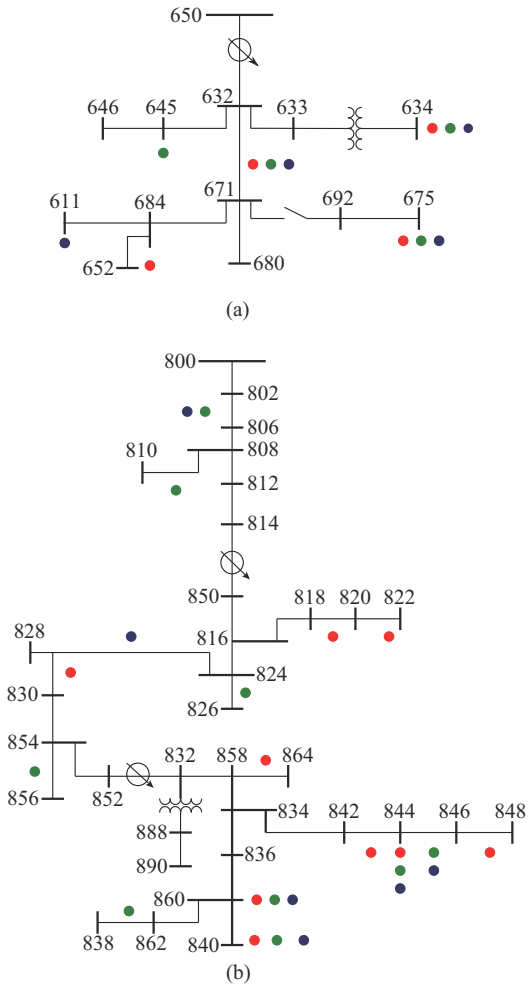

Fig. 6. Distribution network benchmarks used in this study. (a) IEEE 13-bus system. (b) IEEE 34-bus system.

For statistical tests, median values are used. In addition, the obtained results are presented in terms of the following metrics: NCLP, NCL, VES, the amount of injected and consumed reactive power (C_{mode} and L_{mode}), and the optimal placement of ESs. In addition, the correlation of these parameters in the four proposed test scenarios is examined, i.e., 1-4 ESs connected to the power grid. Within each test scenario, the total reactive power threshold for designing the ESs is also contemplated. Finally, once the predominant configuration of the ESs is determined, the influence over distribution network models is considered. Thus, the advantages and disadvantages of the ES capacitive and inductive modes are quantified in terms of the total voltage deviation of the power grid.

VI. RESULTS AND DISCUSSION

The results of the optimal placement of ESs in the IEEE 13-bus and 34-bus systems are presented in this section. The line parameters, power ratings, and load types for both distribution networks are available in [29]. Both systems are characterized by their operation under unbalanced conditions. They consist of single-phase, two-phase, and three-phase feeders, unbalanced loads, and asymmetric distribution lines.

First, the corresponding results for the IEEE 13-bus system, which is characterized by its short length and high load conditions, are described. The high load density provides the opportunity to introduce ESs with high power capacity, which consequently affects the ability to exchange reactive power. In contrast, the IEEE 34-bus system is distinguished by extended length and operation under low load conditions. These specific system conditions offer a greater number of possible placement locations. Furthermore, they enable a comprehensive evaluation of the combined effects of distance and the reactive power capacity of the ES. The method implemented in this study is not restricted to the IEEE 13-bus and 34-bus systems described above. It provides the flexibility to be applicable to any radial distribution network operating under unbalanced conditions.

A. IEEE 13-bus System

Figure 7 shows the GA performance across 31 runs for optimal placement of 1-4 ESs with different Q_t value in IEEE 13-bus system. The performance is presented as a violin plot to show the data distribution, including the median and interquartile ranges. Also, the shape of the plot, resembling a violin, visually represents the frequency of data occurrences, with wider sections indicating a higher density of data points and narrower sections indicating fewer data points. In all test scenarios, $Q_{base}=482.81$ kvar, which corresponds to the maximum reactive power delivered by the ESs when they are simultaneously connected in their 12 possible bus placements. We consider a maximum threshold of 0.4 p.u. with increments of 0.1 p.u. for assessing the impact of reactive power of the ESs on the overall voltage deviation of the distribution network. We use the fitness function according to (13) and a fixed number of iterations, i.e., 20 iterations, as stop criterion of the GA. Each of the points in the figure corresponds to the optimal solution provided by the GA. In this context, the plot form is based only on the distribution of these values, resulting in a testbed of 496 runs. This is equal to 31 errors per Q_t value, considering a range of 1-4 ESs. In addition, the white point indicates the achieved median value for each test.

The results suggest that as long as the Q_t value increases, the voltage deviation, which is associated with the error function, diminishes regardless of the number of ESs. Moreover, the location of an ES obtains the worst mean values for all Q_t (as shown in Fig. 7). Notably, this configuration presents a high data concentration in terms of error minimization, especially for $Q_t=0.3$ and 0.4. This behavior is linked to the fact that a single ES cannot supply all the necessary reactive power for Q_t values. Consequently, there is a slight variation in the error data, exhibiting virtually equal medians. For Q_t of 0.2 p.u., the best median is obtained by combining 2 ESs. It is slightly different (0.99 times) from the error means for 3 and 4 ESs. With respect to Q_t of 0.3 p.u., the disposition of 4 ESs achieves a better average error minimization of 0.07% compared with that in the 2- and 3-ES configurations. Lastly, the best mean mark is achieved for $Q_t=0.4$ p.u., which corresponds to the 3-ES configuration, with a difference of 0.01% compared with that of the 2- and 4-ES configurations.

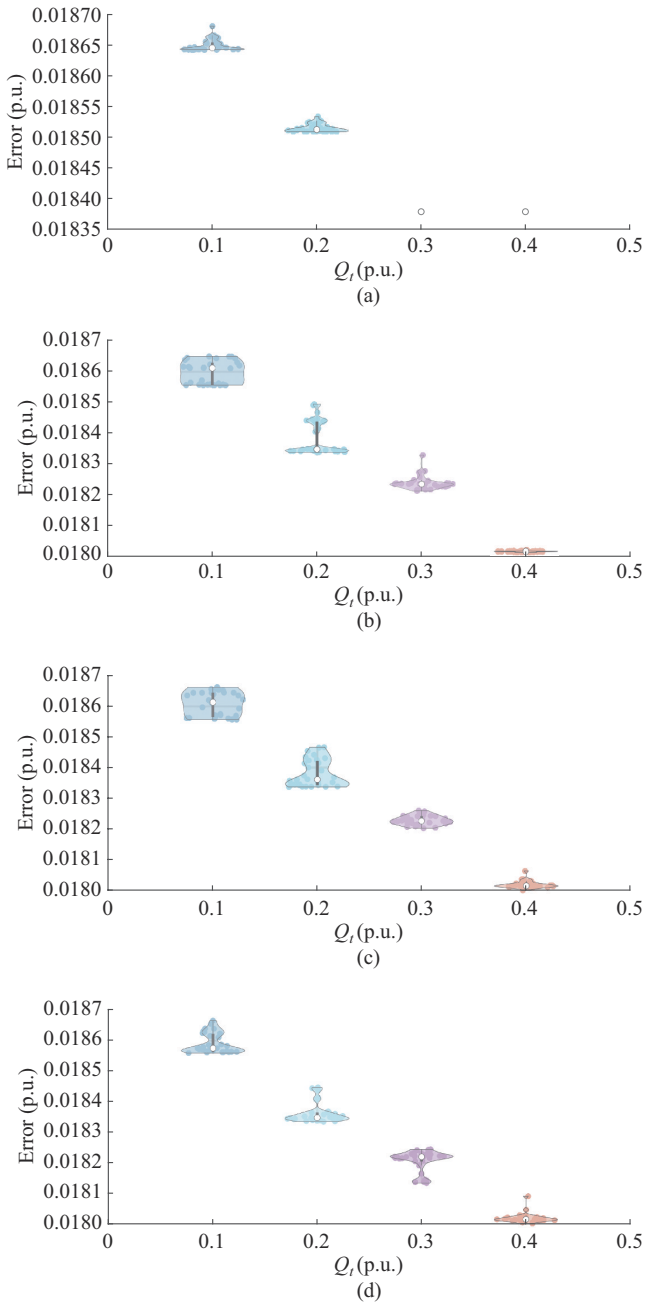

Fig. 7. GA performance across 31 runs for optimal placement of 1-4 ESs with different Q_t value in IEEE 13-bus system. (a) 1 ES. (b) 2 ESs. (c) 3 ESs. (d) 4 ESs.

Table II lists the GA-computed values for different ES configurations with respect to Q_t values. Note that these values are calculated from the medians obtained from the data distribution shown in Fig. 7. The values of column 3, i.e., *NCLP*, are assigned by the GA depending on the number of ESs and the restrictions contemplated in this solver, e.g., $NCLP \leq 0.7$. These values are multiplied by the active power available at the bus and phase where the ES is connected, leading to *NCL* with active power (as shown in column 4 of Table II). Column 5 lists the operational voltage of the ESs computed by the solver (*VES*), which represents a fraction of the rated voltage at the connected bus and is restricted to 0.1-0.6 p.u. to prevent surpassing the nominal voltage at the

connected bus (4160 V). Columns 6 and 7 present the reactive power supplied by the ESs in the capacitive and inductive modes, respectively, given the operating conditions indicated in columns 3 and 5.

TABLMODE II
GA-COMPUTED VALUES FOR DIFFERENT ES CONFIGURATIONS WITH RESPECT TO Q_t VALUES

Configuration	Q_t (p.u.)	*NCLP* (p.u.)	*NCL* (kW)	*VES* (p.u.)	C_{mode} (kvar)	L_{mode} (kvar)	ES position
1 ES	0.1	0.49, -, -, -	142.10, -, -, -	0.40, -, -, -	–48.28, -, -, -	30.19, -, -, -	3
	0.2	0.55, -, -, -	266.75, -, -, -	0.43, -, -, -	–95.56, -, -, -	52.96, -, -, -	1
	0.3	0.70, -, -, -	339.20, -, -, -	0.46, -, -, -	–129.55, -, -, -	68.40, -, -, -	1
	0.4	0.70, -, -, -	339.20, -, -, -	0.46, -, -, -	–129.55, -, -, -	68.40, -, -, -	1
2 ESs	0.1	0.49, 0.20, -, -	329.80, 58.00, -, -	0.10, 0.36, -, -	–30.51, –17.69, -, -	30.21, 11.60, -, -	1, 3
	0.2	0.70, 0.69, -, -	339.50, 200.10, -, -	0.10, 0.39, -, -	–31.04, –65.51, -, -	30.77, 39.59, -, -	1, 3
	0.3	0.69, 0.70, -, -	334.65, 203.00, -, -	0.45, 0.10, -, -	–126.69, –18.14, -, -	67.62, 18.45, -, -	1, 3
	0.4	0.69, 0.70, -, -	334.65, 203.00, -, -	0.44, 0.42, -, -	–123.98, –69.13, -, -	67.84, 40.19, -, -	1, 3
3 ESs	0.1	0.62, 0.20, 0.30, -	300.70, 58.00, 38.40, -	0.10, 0.34, 0.10, -	–27.70, –16.95, –3.61, -	27.46, 11.67, 3.04, -	1, 3, 11
	0.2	0.70, 0.54, 0.46, -	339.50, 156.60, 78.20, -	0.10, 0.42, 0.21, -	–31.05, –54.35, –10.94, -	30.78, 31.32, 10.80, -	1, 3, 11
	0.3	0.67, 0.69, 0.53, -	324.95, 200.10, 63.60, -	0.44, 0.10, 0.10, -	–120.81, –18.16, –5.84, -	65.78, 18.23, 5.84, -	1, 3, 11
	0.4	0.69, 0.69, 0.38, -	334.65, 200.10, 45.60, -	0.42, 0.42, 0.10, -	–120.34, –68.49, –4.27, -	65.82, 39.71, 4.24, -	1, 3, 11
4 ESs	0.1	0.69, 0.43, 0.67, 0.33	334.65, 124.70, 11.39, 39.60	0.10, 0.10, 0.10, 0.10	–31.16, –12.21, –1.09, –3.80	30.83, 12.20, 10.84, 3.79	1, 3, 6, 11
	0.2	0.69, 0.55, 0.29, 0.53	334.65, 159.50, 49.30, 62.10	0.10, 0.43, 0.10, 0.10	–31.07, –54.91, –4.59, –5.91	30.80, 31.51, 4.51, 5.84	1, 3, 4, 8
	0.3	0.42, 0.69, 0.39, 0.69	203.70, 200.10, 6.63, 82.80	0.42, 0.37, 0.10, 0.10	–73.05, –63.33, –0.65, –7.77	41.78, 39.83, 0.65, 7.77	1, 3, 6, 11
	0.4	0.69, 0.69, 0.10, 0.10	203.70, 200.10, 1.70, 22.80	0.43, 0.42, 0.11, 0.10	–121.17, –69.02, –0.19, –2.18	67.69, 40.10, 0.19, 2.17	1, 3, 6, 11

Column 8 presents a condensed overview of the optimal placement analysis for the 4-ES configuration. Notably, positions 1, 3, 4, 6, 8, and 11 correspond to ES placements at buses 675_a, 675_c, 611_c, $632\text{-}671_a$, $632\text{-}671_c$, and 634_c, respectively. The results for optimal placement involving a single ES are detailed in rows 1-4. Bus 675_a is the predominant choice for this setup, appearing in three of the four Q_t values assigned. These operating conditions enable the ES to operate at the highest available power factor at the bus, and the *VES* ensures that the voltage constraints of the *NCL* are not violated. Furthermore, obtaining the same result with Q_t values of 0.3 p.u. and 0.4 p.u. demonstrates that it is not possible to deliver all the required reactive power with a single ES.

Rows 5-8 present the results corresponding to 2 ESs. Note that for all Q_t values, the GA detects the optimal placements of ES at buses 675_a and 675_c. For a Q_t value of 0.1 p.u., the GA adjusts *NCLP* and *VES* to distribute the reactive power between both devices without reaching their limiting values. Subsequently, the GA assigns *NCLP* close to the maximum for both ESs (*NCLP* = 0.7) and adjusts *VES* to modify the reactive power of each ES. In the 3-ES configuration, an ES is added to bus 634_c by preserving the ESs at bus 675 (as shown in rows 9-12). This new ES has the minimum impact on the overall reactive power, contributing only 6.26% in the capacitive mode and 8.09% in the inductive mode on average for the different Q_t values. The 4-ES configuration exhibits a similar behavior, where the contributions of the new placements to the predominant synergy is the minimum in terms of the overall reactive power (as shown in rows 13-16 of Table II). For instance, the ES at bus 634_c contributes a mean of 5.12% in the capacitive mode and 6.30% in the inductive mode. Meanwhile, the ES at bus $632\text{-}671_a$ contributes a mean of 1.88% and 6.47% for capacitive and inductive modes, respectively. Thus, the placement of ESs in 675_a and 675_c clearly has the greatest impact on voltage deviation. This can be attributed to multiple influential factors, including the fact that bus 675 is one of the farthest points in the distribution network and that it has a high load concentration, which significantly affects both NCL and ES power requirements. Furthermore, because of the nonuniform load distribution and unbalanced operating conditions within the IEEE 13-bus system, phases *a* and *c* experience more pronounced voltage deviations, which necessitate specific attention and corrective measures.

Figure 8 shows the total voltage deviation per phase in IEEE 13-bus system, including the 4-ES configuration and a Q_t value of 0.4 (as shown in row 16 of Table II). In the absence of any ES, denoted by the red curve, the base case voltage profile is obtained. Moreover, the voltage profile during ES operation at the maximum power in the capacitive mode is shown in yellow, and the profile for the inductive mode operation is represented in blue. This visual representation demonstrates the impact of the ES operation on the voltage profile within the IEEE 13-bus system. Therefore, what appears to be a deterioration in voltage deviation should be interpreted as the suppressive action capacity of the ESs on that specific phase. Conversely, an enhancement in voltage deviation indicates the ability of the ESs to offer voltage support. Note that we avoid the ES connections at buses 646, 671, and 692 because their load configuration is delta-type. Notwithstanding, for this analysis, we consider the impact of ESs on these buses. Figure 8(a) shows the typical behavior of ESs, providing voltage support in the capacitive mode and voltage suppression in the inductive mode. Nonetheless, the effects of grid magnetic couplings, load imbalances, and

the capacity of ESs to supply and consume the reactive power may lead to a distinct outcome in the remaining grid phases. Additionally, ES can supply reactive power rather than consume it, as shown in columns 6 and 7 of Table II.

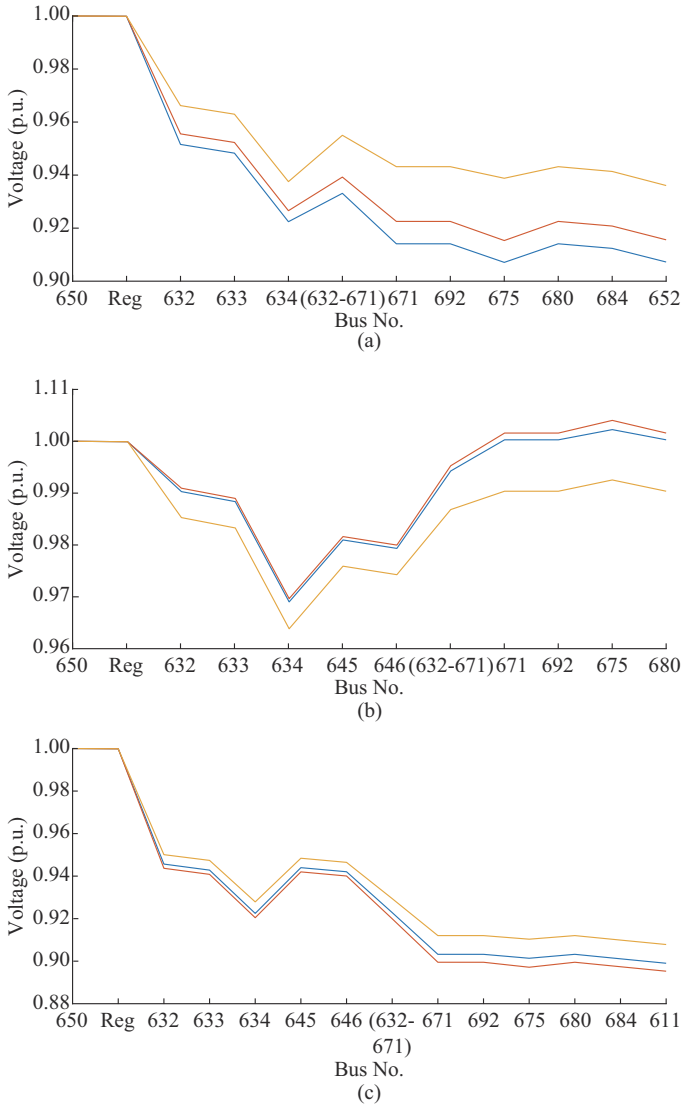

Fig. 8. Total voltage deviation per phase in IEEE 13-bus system. (a) Phase *a*. (b) Phase *b*. (c) Phase *c*.

Phase *b* behaves in the opposite manner compared with phase *a* (in capacitive mode). A similar phenomenon arises in phase *c*, in which the inductive mode has limited ability to absorb reactive power. Nonetheless, the inductive and capacitive modes depict the expected behavior for phases *b* and *c*, respectively. The reason is twofold. The first reason is that most ESs are distributed between grid phases *a* and *c* (as shown in column 8 of Table II). The second reason is the amount of reactive power interchanges between the ESs and the distribution network (as shown in columns 6 and 7 of Table II). With regard to the voltage deviation in the base case, i.e., without ESs, average voltage deviations of 0.9411, 0.9929, and 0.9282 p.u. are obtained for phases *a*, *b*, *c*, respectively. In the capacitive and inductive modes, the ESs cause median voltage deviations of 0.9556, 0.9861, 0.9368 p.u. and 0.9354, 0.9921, 0.9308 p.u. per phase. Based on the average voltage deviations, it can be observed that the IEEE 13-bus system has a voltage deviation range of up to 2.02% for phase *a* and 0.6% for phases *b* and *c*, respectively.

B. IEEE 34-bus System

To complement our method, we assess the GA performance in the IEEE 34-bus system. In this case study, a Q_{base} of 183.92 kvar is calculated by operating the ESs in all 24 possible placements at their maximum reactive power. We follow the same analysis as in the case of the IEEE 13-bus system. For brevity, we neglect the results corresponding to $Q_t = 0.1$ because the data distribution for each ES presents a low variation, which visually does not reveal significant information. Likewise, this configuration yields the worst median marks for all Q_t values. Figure 9 shows the GA performance across 31 runs for optimal placement of 1-4 ESs with different Q_t values, where a violin plot is also used. The trend is clear: the best mean values are obtained when $Q_t =$ 0.4 p.u., regardless of the number of ESs. In quantitative terms, these values have an average error minimization, which is 0.99 times better than those achieved in the cases when $Q_t = 0.2$ and 0.3.

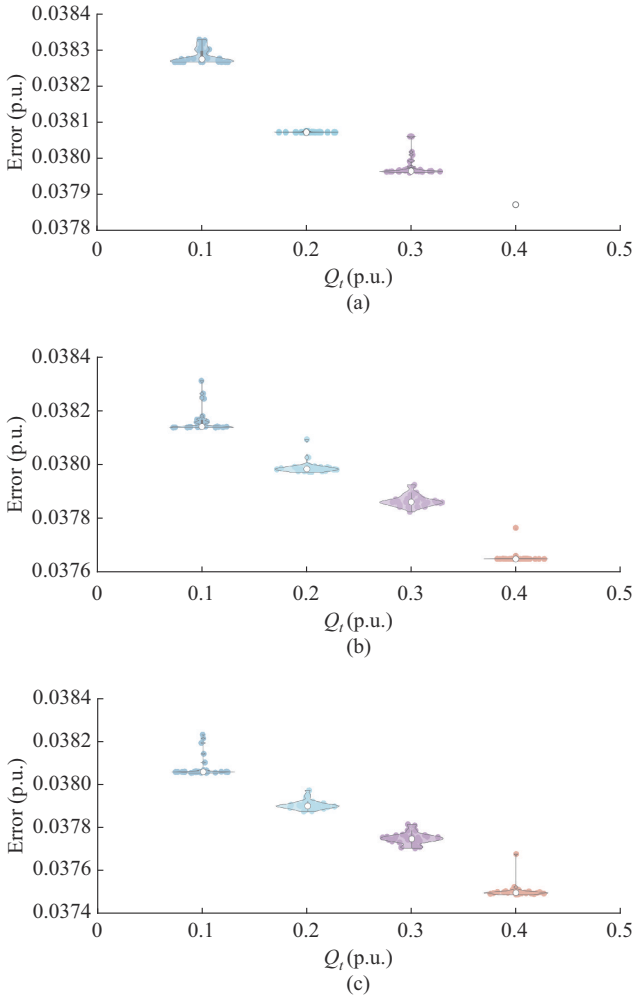

Fig. 9. GA performance across 31 runs for optimal placement of 1-4 ESs with different Q_t in IEEE 34-bus system. (a) 2 ESs. (b) 3 ESs. (c) 4 ESs.

Positions 1, 5, 8, 9, 12, and 20 correspond to ES placements at buses 862-838$_b$, 860$_a$, 846-848$_b$, 844-846$_b$, 844$_b$ and 820-822$_a$, respectively. In the single-ES configuration, the optimal placement consistently aligns with bus 820-822$_a$, regardless of the Q_t values. This particular bus is strategically positioned within the central region of the distribution network and has an available active power capacity of 135 kW, which is 22.27% of the total power in phase *a* of the power network. The highest NCL active power is achieved starting from $Q_t = 0.2$ p.u. with a value of 94.5 kW, allowing injection of up to −31.55 kvar in the capacitive mode and 15.15 kvar in the inductive mode. In the 2-ES configuration, there are two predominant setups that include buses 820-822$_a$ (as shown in rows 5 to 8). For low Q_t values (0.1 p.u. and 0.2 p.u.), a second ES is added at bus 862-838$_b$. Given the available active power at this bus, this ES can operate with an NCL of up to 19.6 kW, allowing for a maximum exchange of reactive power of −6.01 kvar in the capacitive mode and 4.52 kvar in the inductive mode. Although this reactive power capacity is one-fifth of that of ES with buses 820-822$_a$, the ES placement at the farthest point of the distribution network has a significant impact on voltage deviation. Conversely, when increasing the Q_t value to 0.3 and 0.4, it becomes necessary for the ESs to deliver more power, and hence, the second ES is placed at bus 844$_b$. This change is directly related to the amount of active power available at this bus, which is 135 kW. This value corresponds to 23.11% of all the available power in phase *b* of the distribution network, allowing the ES to operate with an NCL of up to 94.5 kW. Notably, for the 3- and 4-ES configurations, a similar pattern emerges where the ES at bus 844$_b$ is included for Q_t values of 0.3 p.u. and 0.4 p.u. because of the need for a greater exchange of reactive power. Instead, for low Q_t values, the emphasis is on the placement farther along the feeder, even if the available active power is lower. This is the case for the ESs located at buses 844-846$_b$, 860$_a$, and 846-848$_b$, which have active power ratings of 25 kW, 20 kW, and 23 kW, respectively.

Figure 10 provides a visual representation of the total voltage deviation per phase in IEEE 34-bus system. The red curve denotes the base case voltage profile, reflecting conditions without ES operation. The yellow curve represents the voltage profile when the ESs are operating at their maximum power in the capacitive mode, and the blue curve showcases the voltage profile under conditions where the ESs are operating at their maximum power in the inductive mode. The operating parameters and ES placement for this specific case study correspond to the data presented in row 16 of Table III. This graphical representation effectively conveys how the operation of ESs affects the voltage profile within the IEEE 34-bus system. For this case, Fig. 10(b) shows the expected outcome of the capacitive and inductive modes of the ESs plugged into the power grid. This is because three of four optimal placements of ES found by the GA belong to phase *b*. The remaining positions are designated to phase *a* (as shown in Fig. 10(a)), which also achieves the effect desired solely for the ESs operating in the capacitive mode. However, in the inductive mode of this phase, voltage reduction is not achieved. Likewise, both modes in phase *c* show the opposite effect in accordance with what happened in phase *b* (as shown in Fig. 10(c)), which is intimately connected to the magnetic coupling within the distribution lines. This finding illustrates that the substantial concentration of ESs in phase *b* and the placement of a high power ES in phase *a* affect voltage regulation at their respective buses and connection phases, and have a repercussion across the other phases. An anomalous operational effect becomes apparent in phase *c*, which is primarily attributed to the absence of ESs in that phase. Thus, the base case has average voltage deviations of 0.8795, 0.9145, and 0.9163 p.u. for phases *a*, *b*, and *c*, respectively. Moreover, the capacitive mode achieves the mean voltage deviations of 0.8868, 0.9264, and 0.9141 p.u. for phases *a*, *b*, and *c*, respectively, while the inductive mode achieves the mean voltage deviations of 0.8843, 0.9120, 0.9162 p.u. for phases *a*, *b*, and *c*, respectively. Hence, the IEEE 34-bus system shows an average voltage deviation range of 0.25% for phase *a*, 1.44% for phase *b*, and 0.21% for phase *c*.

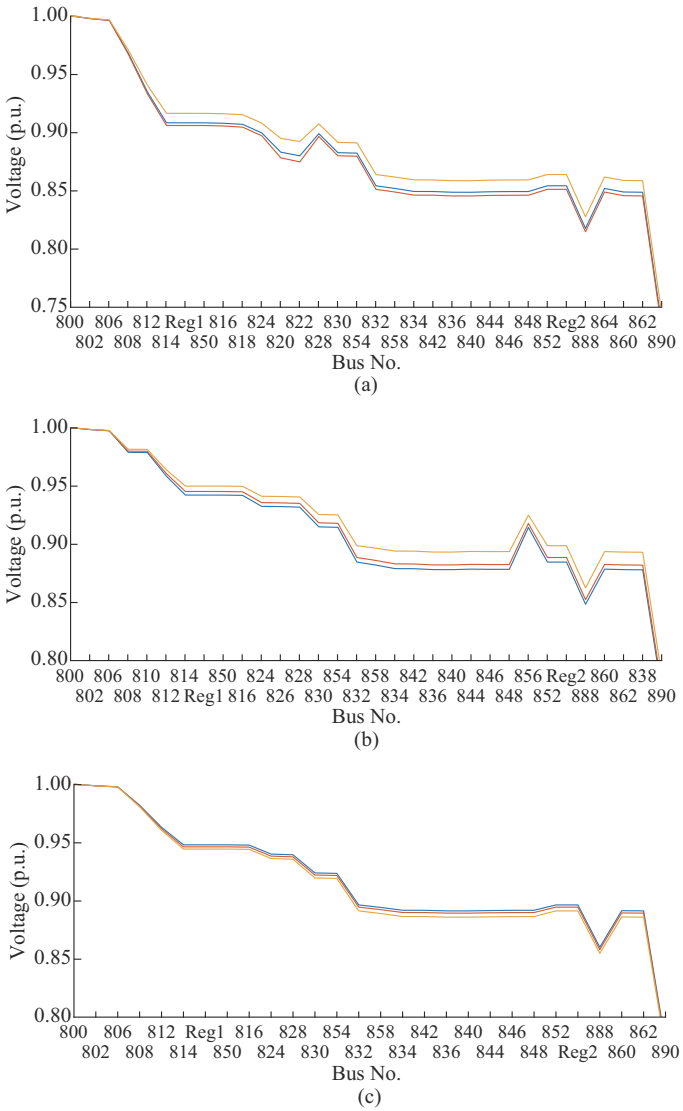

Fig. 10. Total voltage deviation per phase in IEEE 34-bus system. (a) Phase *a*. (b) Phase *b*. (c) Phase *c*.

TABLE III
ES CONFIGURATION TAKEN FROM MEDIAN VALUES OF FIG. 9

Configuration	Q_t (p.u.)	*NCLP* (p.u.)	*NCL* (kW)	*VES* (p.u.)	C_{mode} (kvar)	L_{mode} (kvar)	ES position
1 ES	0.1	0.70, -, -, -	94.50, -, -, -	0.22, -, -, -	−18.39, -, -, -	17.15, -, -, -	20
	0.2	0.70, -, -, -	94.50, -, -, -	0.42, -, -, -	−31.55, -, -, -	17.15, -, -, -	20
	0.3	0.70, -, -, -	94.50, -, -, -	0.42, -, -, -	−31.55, -, -, -	17.15, -, -, -	20
	0.4	0.70, -, -, -	94.50, -, -, -	0.42, -, -, -	−31.55, -, -, -	17.15, -, -, -	20
2 ESs	0.1	0.70, 0.70, -, -	19.60, 94.50, -, -	0.39, 0.14, -, -	−5.64, −12.74, -, -	4.52, 12.66, -, -	1, 20
	0.2	0.70, 0.70, -, -	19.60, 94.50, -, -	0.38, 0.41, -, -	−6.01, −30.76, -, -	4.52, 17.16, -, -	1, 20
	0.3	0.66, 0.70, -, -	89.10, 94.50, -, -	0.40, 0.33, -, -	−29.00, −26.16, -, -	20.66, 17.20, -, -	12, 20
	0.4	0.70, 0.70, -, -	94.50, 94.50, -, -	0.40, 0.42, -, -	−30.59, −31.34, -, -	21.75, 17.20, -, -	12, 20
3 ESs	0.1	0.70, 0.69, 0.69, -	19.60, 17.25, 93.15, -	0.26, 0.39, 0.10, -	−4.39, −5.50, −8.48, -	4.37, 4.07, 8.46, -	1, 9, 20
	0.2	0.70, 0.70, 0.70, -	19.60, 17.25, 94.50, -	0.14, 0.39, 0.37, -	−2.42, −5.45, −28.91, -	2.41, 4.07, 17.17, -	1, 9, 20
	0.3	0.70, 0.61, 0.70, -	19.60, 82.35, 94.50, -	0.10, 0.40, 0.33, -	−1.74, −27.00, −26.42, -	1.71, 19.21, 17.21, -	1, 12, 20
	0.4	0.70, 0.70, 0.70, -	19.60, 94.50, 94.50, -	0.41, 0.41, 0.42, -	−6.48, −31.31, −31.31, -	4.49, 21.79, 17.22, -	1, 12, 20
4 ESs	0.1	0.70, 0.70, 0.70, 0.70	19.60, 14.00, 17.50, 94.50	0.33, 0.10, 0.23, 0.10	−5.42, −1.18, −3.46, −8.30	4.52, 1.18, 3.45, 8.27	1, 5, 9, 20
	0.2	0.70, 0.69, 0.69, 0.67	19.60, 15.87, 17.25, 90.45	0.10, 0.38, 0.10, 0.38	−1.77, −4.98, −1.64, −28.29	1.76, 3.74, 1.64, 16.66	1, 8, 9, 20
	0.3	0.69, 0.70, 0.34, 0.70	19.32, 17.50, 45.90, 94.50	0.33, 0.35, 0.40, 0.39	−5.45, −5.05, −15.00, −29.65	4.50, 4.05, 10.81, 17.21	1, 9, 12, 20
	0.4	0.70, 0.69, 0.69, 0.69	19.60, 17.25, 93.15, 93.15	0.42, 0.36, 0.42, 0.40	−6.55, −5.24, −31.37, −30.37	4.50, 4.02, 21.64, 17.22	1, 9, 12, 20

VII. CONCLUSION

A novel planning tool is proposed for optimizing the placement of ESs in unbalanced distribution networks. Based on GA and BFSM, the most suitable grid buses to connect ESs are identified. Moreover, the ES operation modes and their effects on both distribution models are analyzed. These effects are quantified using the total voltage deviation of the power grid. To achieve optimal ES operation, the proposed method adopts realistic restrictions for the NCLP and VES parameters, which directly affect the NCL values and the ES capacity to inject and consume reactive power.

In the IEEE 13-bus system, 675_a and 675_c consistently emerge as the prominent choices in different configurations. The observation agrees with the fact that the particular bus is one of the farthest points in the distribution network, which has the highest available active power. In contrast, the IEEE 34-bus system exhibits a different pattern, seeking a balance between placements with the highest available active power and distance from buses in the distribution network. $820\text{-}822_a$ consistently remains the primary choice in all configurations owing to its superior available active power compared with other buses. In scenarios with multiple ESs, the ESs tend to be distributed to the farthest buses in the network when Q_t has low values (0.1 and 0.2). However, for higher Q_t values (0.3 and 0.4), the optimal placement shifts, favoring a bus with greater available active power, such as 844_b. The phases with a higher concentration of ESs exhibit the typical behavior of providing voltage support in the capacitive mode and voltage suppression in the inductive mode, while the phases without ESs exhibit the opposite behavior. This behavior is a result of the asymmetric injection of reactive power by ESs and the unbalanced operating conditions of the distribution network. Although excellent results have been obtained, it is necessary, as future work, to address some of the research constraints and opportunities identified in the present study. These include extending the method to other grid topologies, proposing schemes to improve computational time, and individually or jointly evaluating other power quality metrics and their impact on the optimal placement of ESs.

REFERENCES

[1] B. Ahmadi, J. S. Giraldo, G. Hoogsteen *et al*., "A multi-objective decentralized optimization for voltage regulators and energy storage devices in active distribution systems," *International Journal of Electrical Power & Energy Systems*, vol. 153, pp. 1-14, Nov. 2023.

[2] O. Babayomi, Z. Zhang, T. Dragicevic *et al*., "Smart grid evolution: predictive control of distributed energy resources – a review," *International Journal of Electrical Power & Energy Systems*, vol. 147, pp. 1-20, May 2023.

[3] M. S. Alam, F. S. Al-Ismail, A. Salem *et al*., "High-level penetration of renewable energy sources into grid utility: challenges and solutions," *IEEE Access*, vol. 8, pp. 1-23, Oct. 2020.

[4] M. Zanganeh, M. S. Moghaddam, A. Azarfar *et al*., "Multi-area distribution grids optimization using D-FACTS devices by M-PSO algorithm," *Energy Reports*, vol. 9, pp. 133-147, Dec. 2023.

[5] V. Vijayan, A. Mohapatra, and S. Singh, "Demand response with volt/var optimization for unbalanced active distribution systems," *Applied Energy*, vol. 300, pp. 1-14, Oct. 2021.

[6] C. Huang, H. Zhang, Y. Song *et al*., "Demand response for industrial micro-grid considering photovoltaic power uncertainty and battery operational cost," *IEEE Transactions on Smart Grid*, vol. 12, no. 4, pp. 3043-3055, Jul. 2021.

[7] C. K. Lee, B. Chaudhuri, and S. Hui, "Hardware and control implementation of electric springs for stabilizing future smart grid with intermittent renewable energy sources," *IEEE Journal of Emerging and Selected Topics in Power Electronics*, vol. 1, pp. 18-27, Mar. 2013.

[8] G. Tapia-Tinoco, A. Garcia-Perez, D. Granados-Lieberman *et al*., "Hardware structures, control strategies, and applications of electric springs: a state-of-the-art review," *IET Generation, Transmission & Distribution*, vol. 14, pp. 5349-5363, Oct. 2020.

[9] D. A. Quijano, A. Padilha-Feltrin, and J. P. S. Catalão, "Probabilistic rolling-optimization control for coordinating the operation of electric springs in microgrids with renewable distributed generation," *IEEE Transactions on Sustainable Energy*, vol. 13, no. 4, pp. 2159-2171, Oct. 2022.

[10] Y. Zheng, D. J. Hill, K. Meng *et al*., "Critical bus voltage support in

distribution systems with electric springs and responsibility sharing," *IEEE Transactions on Power Systems*, vol. 32, no. 5, pp. 3584-3593, Sept. 2017.
[11] J. Wang, K. Lao, N. Dai *et al*., "A low-order steady-state model of electric springs for conservation voltage reduction in active distribution networks with renewables," *IEEE Transactions on Power Delivery*, vol. 39, no. 1, pp. 1-14, Nov. 2022.
[12] C.-K. Lee, H. Liu, S.-C. Tan *et al*., "Electric spring and smart load: technology, system-level impact, and opportunities," *IEEE Journal of Emerging and Selected Topics in Power Electronics*, vol. 9, pp. 6524-6544, Dec. 2021.
[13] P. Li, H. Ji, C. Wang *et al*., "Optimal operation of soft open points in active distribution networks under three-phase unbalanced conditions," *IEEE Transactions on Smart Grid*, vol. 10, no. 1, pp. 380-391, Jan. 2019.
[14] S. Gupta and K. Deep, "An efficient grey wolf optimizer with opposition-based learning and chaotic local search for integer and mixed-integer optimization problems," *Arabian Journal for Science and Engineering*, vol. 44, pp. 1-20, Apr. 2019.
[15] E. Hadian, H. Akbari, M. Farzinfar *et al*., "Optimal allocation of electric vehicle charging stations with adopted smart charging/discharging schedule," *IEEE Access*, vol. 8, pp. 1-12, Oct. 2020.
[16] A. Ali, M. U. Keerio, and J. A. Laghari, "Optimal site and size of distributed generation allocation in radial distribution network using multi-objective optimization," *Journal of Modern Power Systems and Clean Energy*, vol. 9, no. 2, pp. 404-415, Mar. 2021.
[17] M. R. Nayak, D. Behura, and K. Kasturi, "Optimal allocation of energy storage system and its benefit analysis for unbalanced distribution network with wind generation," *Journal of Computational Science*, vol. 51, pp. 1-10, Apr. 2021.
[18] Y. Zheng, D. J. Hill, Y. Song *et al*., "Optimal electric spring allocation for risk-limiting voltage regulation in distribution systems," *IEEE Transactions on Power Systems*, vol. 35, no. 1, pp. 273-283, Jan. 2020.
[19] L. Liang, H. Yi, Y. Hou *et al*., "An optimal placement model for electric springs in distribution networks," *IEEE Transactions on Smart Grid*, vol. 12, no. 1, pp. 491-501, Jan. 2021.
[20] J. Han, N. Liu, and J. P. S. Catalão, "Optimization of distribution network and mobile network with interactive balance of flexibility and power," *IEEE Transactions on Power Systems*, vol. 38, no. 3, pp. 2512-2524, May 2023.
[21] G. Tapia-Tinoco, D. Granados-Lieberman, M. Valtierra-Rodriguez *et al*., "Modeling of electric springs and their multi-objective voltage control based on continuous genetic algorithm for unbalanced distribution networks," *International Journal of Electrical Power & Energy Systems*, vol. 138, p. 107979, Jun. 2022.
[22] G. H. Valencia-Rivera, M. T. Benavides-Robles, A. V. Morales *et al*., "A systematic review of metaheuristic algorithms in electric power systems optimization," *Applied Soft Computing*, vol. 150, pp. 1-14, Jan. 2024.
[23] S. H. C. Cherukuri and B. Saravanan, "Hybrid energy management strategy for residential consumers using virtual and actual storage systems," *Journal of Energy Storage*, vol. 25, pp. 1-14, Oct. 2019.
[24] E. F. Areed, M. A. Abido, and A. T. Al-Awami, "Switching model analysis and implementation of electric spring for voltage regulation in smart grids," *IET Generation, Transmission & Distribution*, vol. 11, pp. 3703-3712, Jun. 2017.
[25] V. Chahar, S. Katoch, and S. Chauhan, "A review on genetic algorithm: past, present, and future," *Multimedia Tools and Applications*, vol. 80, pp. 8091-8126, Oct. 2020.
[26] Z. Akhtar, B. Chaudhuri, and S. Y. R. Hui, "Smart loads for voltage control in distribution networks," *IEEE Transactions on Smart Grid*, vol. 8, no. pp. 937-946, Mar. 2017.
[27] Y. Zheng, W. Kong, Y. Song *et al*., "Optimal operation of electric springs for voltage regulation in distribution systems," *IEEE Transactions on Industrial Informatics*, vol. 16, no. pp. 2551-2561, Apr. 2020.
[28] L. Liang, Y. Hou, D. J. Hill *et al*., "Enhancing resilience of microgrids with electric springs," *IEEE Transactions on Smart Grid*, vol. 9, no. pp. 2235-2247, May 2018.
[29] I. P. & Society. (2023, Apr.). IEEE PES DSACOM. [Online]. Available: https://cmte.ieee.org/pes-testfeeders/resources/

Guillermo Tapia-Tinoco received the B.S. and M.Sc. degrees in electrical engineering from the Michoacan University of Saint Nicholas of Hidalgo (UMSNH), Morelia, Mexico, and the Ph.D. degree in electrical engineering from the University of Guanajuato (UG), Irapuato, Mexico. He is currently a part-time Professor in the Department of Agricultural Engineering at UG and a National Researcher Level 1 of the Mexican Council of Science and Technology. His research interests include application of artificial intelligence algorithm to active distribution network.

Gerardo Humberto Valencia-Rivera received the B.Sc. degree in mechatronics from the Universidad Santo Tomás, Bucaramanga, Colombia, in 2017, and the M.Sc. degree in electrical engineering from the Universidad of Guanajuato, Salamanca, Mexico, in 2019. He is currently pursuing the doctoral degree in computer science at Tecnológico de Monterrey, Monterrey, México. His research interests include optimal control, microgrid, power quality, metaheuristics, and hyper-heuristics.

Martin Valtierra-Rodriguez received the B.E. degree in mechatronics engineering and M.E. degree in electrical engineering from the University of Guanajuato, Salamanca, Mexico, and the Ph.D. degree in mechatronics from the Autonomous University of Queretaro, San Juan del Río, Mexico. He is currently a Full Professor at the Faculty of Engineering, Autonomous University of Queretaro. He is also a Level 2 Member of the Mexican National Research System (SNII). His research interests include fault detection and condition monitoring of electrical and mechanical systems using signal processing and artificial intelligence.

Arturo Garcia-Perez received the Ph.D. degree in electrical engineering from The University of Texas at Dallas, Pallas, USA, in 2005. He is currently a Full Professor at the University of Guanajuato, Salamanca, Mexico. He is a National Researcher Level 3 of the Mexican Council of Science and Technology. His research interests include signal processing, spectral analysis, and monitoring and diagnosis of power system.

David Granados-Lieberman received the B.E. and M.E. degrees from the University of Guanajuato, Salamanca, Mexico, and the Ph.D. degree from the Autonomous University of Queretaro, San Juan del Río, Mexico. He is currently a Professor with the Electromechanical Engineering Department of the National Technological Institute of Mexico/ITS Irapuato, Irapuato, Mexico. He is a Level 2 Member of the Mexican National Research System (SNII). His current research interests include power system analysis, signal processing, and mechatronics.